

# Bayesian approach to gravitational lens model selection: constraining $H_0$ with a selected sample of strong lenses

I. Balmès<sup>1\*</sup> & P.S. Corasaniti<sup>1</sup>

<sup>1</sup>CNRS, Laboratoire Univers et Théories (LUTH), UMR 8102 CNRS, Observatoire de Paris, Université Paris Diderot, 5 Place Jules Janssen, 92190 Meudon, France

## ABSTRACT

Bayesian model selection methods provide a self-consistent probabilistic framework to test the validity of competing scenarios given a set of data. We present a case study application to strong gravitational lens parametric models. Our goal is to select a homogeneous lens subsample suitable for cosmological parameter inference. To this end we apply a Bayes factor analysis to a synthetic catalog of 500 lenses with power-law potential and external shear. For simplicity we focus on double-image lenses (the largest fraction of lens in the simulated sample) and select a subsample for which astrometry and time-delays provide strong evidence for a simple power-law model description. Through a likelihood analysis we recover the input value of the Hubble constant to within  $3\sigma$  statistical uncertainty. We apply this methodology to a sample of double image lensed quasars. In the case of B1600+434, SBS 1520+530 and SDSS J1650+4251 the Bayes' factor analysis favors a simple power-law model description with high statistical significance. Assuming a flat  $\Lambda$ CDM cosmology, the combined likelihood data analysis of such systems gives the Hubble constant  $H_0 = 76_{-5}^{+15} \text{ km s}^{-1} \text{ Mpc}^{-1}$  having marginalized over the lens model parameters, the cosmic matter density and consistently propagated the observational errors on the angular position of the images. The next generation of cosmic structure surveys will provide larger lens datasets and the method described here can be particularly useful to select homogeneous lens subsamples adapted to perform unbiased cosmological parameter inference.

**Key words:** cosmology: observations - cosmology: theory

## 1 INTRODUCTION

Strong gravitational lenses are powerful cosmological probes. The distorted images of lensed background sources carry information on the distribution of invisible matter in cosmic structures. Furthermore, as light-rays from distant variable sources propagate along differently distorted paths, time-delays between luminosity variations of the source images test the underlying cosmological expansion (for exhaustive review see Schneider, Ehlers & Falco 1991; Petters, Levine & Wambsganss 2001; Schneider, Kochanek & Wambsganss 2006).

The use of lens time-delays as cosmic standard rulers was initially proposed by Refsdal (1964, 1966). To date time-delays have been measured only in 21 lensed quasars out of the few hundreds known strong lens systems. Despite the scarcity of observations, lots of effort has been devoted to using these data to infer the value of the Hubble constant,  $H_0$ . This is because time-delays, differently from other standard cosmological tests, do not rely on local calibration measurements, such as the distance ladder method (for an alternative method see Chavez et al. 2012). In the next decade, additional lens time-delay data will become available thanks to obser-

vational programs such as the COSMOGRAIL<sup>1</sup> project collaboration, as well as the ILMT project<sup>2</sup>. Furthermore, the next generation of cosmic structure surveys such as the Dark Energy Survey (DES), the Large Synoptic Telescope (LSST) or the EUCLID satellite mission will detect large sample of strong lens systems for which time-delays can be accurately measured through follow-up observations. Time-delays from such datasets will be particularly useful to infer cosmological constraints that are complementary to those obtained from other cosmic probes (see e.g. Dobke et al. 2009; Coe & Moustakas 2009; Oguri & Marshall 2010; Linder 2011).

Time-delay measurements are particularly challenging because they require an intense monitoring of the lens system. However, the main limitation to fully exploit the cosmological information encoded in such data arises from the uncertainty on the lens mass distribution as well as the presence of perturbing masses along the line-of-sight. Because of this, several analyses have focused on “golden lenses” (Press 1996; Williams & Schechter 1997). These are systems for which there is a sufficient number of observational features (e.g. presence of arcs, multiple point-like images, flux ra-

<sup>1</sup> <http://www.cosmograil.org>

<sup>2</sup> <http://www.aeos.ulg.ac.be/LMT/index.php>

\* E-mail: Irene.Balmes@obspm.fr

tios measurements) such as to constrain the lens potential independently of time-delays. For example, Wucknitz, Biggs & Browne (2004) have studied the lens system B0218+357 and inferred  $H_0 = 78 \pm 6 \text{ km s}^{-1} \text{ Mpc}^{-1}$  for a flat Cold Dark Matter model with Cosmological Constant ( $\Lambda$ CDM) with mean matter density  $\Omega_m = 0.3$ . Suyu et al. (2010) have analysed the lens B1608+656 and for the same cosmology they have obtained  $H_0 = 70.6 \pm 3.1 \text{ km s}^{-1} \text{ Mpc}^{-1}$ .

Alternatively one can infer cosmological parameter constraints using a statistical sample of lens time-delay measurements (see e.g. Saha et al. 2006; Oguri 2007). Such an approach still requires modeling the gravitational potential of each lens in the sample. Nevertheless, one can hope that systematics due to individual mass model uncertainties are averaged out. In such a case sample selection effects can be the main source of error (Oguri, Keeton & Dalal 2005; Oguri 2006).

Modeling the lens mass distribution can be distinguished in parametric (e.g. see Oguri 2002; Keeton, Gaudi & Petters 2003; Oguri 2007) and non-parametric (e.g. see Kochanek 1991; Saha & Williams 1997; Koopmans 2005; Vegetti & Koopmans 2009; Suyu et al. 2009) methods. The latter uses linear inversion algorithms to constrain the lens potential directly from the intensity images of the lens system, while the former uses the measured properties of the lens to constrain a parametrized form of the lens potential. A third approach by Alard (2007, 2008) reconstructs the lens potential as a perturbative expansion around the Einstein ring of the lens system.

Non-parametric methods have been extensively used in a vast literature. As an example a non-parametric reconstruction algorithm is implemented in Pixelens<sup>3</sup> (Williams & Saha 2000), a numerical code commonly used for lens studies. Using this code Saha et al. (2006) have found  $H_0 = 72_{-11}^{+8} \text{ km s}^{-1} \text{ Mpc}^{-1}$  from a sample of 10 time-delay lenses for a flat  $\Lambda$ CDM with  $\Omega_m = 0.3$ . Recently Paraficz & Hjorth (2010) have performed the same analysis on an extended sample of 18 lenses and obtained  $H_0 = 66_{-4}^{+6} \text{ km s}^{-1} \text{ Mpc}^{-1}$ . A statistical analysis of a sample of lensed quasars using a parametric approach has been performed by a number of authors. For instance, assuming an isothermal lens potential Giovi & Amendola (2001) have inferred limits on  $H_0$  for different cosmological models. The analysis by Oguri (2007) has propagated the uncertainties in the lens model parameters and found  $H_0 = 70 \pm 6 \text{ km s}^{-1} \text{ Mpc}^{-1}$  from a sample of 16 lenses for a flat  $\Lambda$ CDM with  $\Omega_m = 0.26$ . Whether using non-parametric lens reconstruction algorithms or a parametric model a key aspect of these analyses is the assessment of what constitutes a good description of the lens potential given the data.

Independently of the approach used, distinguishing between the potentially infinite number of possibilities has been mostly based on  $\chi^2$ -statistics. However, parameter fitting only establishes how well a model reproduce the data for a given set of model parameter values. Deciding whether one model is preferable over another is a question of *model selection* rather than quality of parameter fit. In other words, which model has a higher probability of being the correct model description of the observations? Do the data justify a more complex description of the system (additional parameters)?

In the Bayesian statistical framework these questions are addressed by the analysis of the Bayesian evidence and the evaluation of Bayes factor (Jeffreys 1961; MacKay 2003; Gregory

2005). Bayesian model selection methods have already been applied to a variety of problems in cosmology and astrophysics (e.g. see Jaffe 1996; Marshall, Hobson & Slosar 2003; Saini et al. 2004; Bassett, Corasaniti & Kunz 2008; Mukherjee, Parkinson & Liddle 2006; Mukherjee et al. 2006; Trotta 2007; Ford & Gregory 2007; Cornish & Littenberg 2007; Gregory & Fischer 2010). In the literature, the analysis of Bayes factors has been applied to non-parametric lens reconstruction techniques (Suyu et al. 2006; Vegetti & Koopmans 2009) as well as selecting complicate parametric lens models of galaxy clusters (Jullo et al. 2007).

Here, we present a case study of the use of Bayes factors to construct a homogeneous sample of double lensed quasars to derive bounds on  $H_0$ . By homogeneous we mean a sample consisting of lenses whose data, astrometry and time-delays of the images, provide evidence for the same lens model description at the same level of statistical significance. Differently from previous statistical approaches we consistently propagate all observational uncertainties on the posterior probabilities, including errors on the angular position of the images, as well as marginalizing over nuisance model parameters rather than assuming hard priors. The possibility of selecting homogeneous lens data to infer cosmological parameter constraints will become particularly important for future survey programs which will detect a large number of strong gravitational lenses. We argue that the use of Bayes factors provides a self-consistent probabilistic method to build subsample of data which are not dominated by astrophysical selection effects.

The paper is organized as follows: in Section 2 we review the lens equations and the modeling of the gravitational lens potential, while in Section 3 we discuss the Bayesian model selection. We present the results of the lens model selection analysis on simulated data in Section 4 and on real data in Section 5. In Section 6 we describe the results of the cosmological parameter inference and present our conclusions in Section 7.

## 2 GRAVITATIONAL LENSES

### 2.1 Lens equations

Here, we briefly review the basic equations describing the formation of images in strong gravitational lenses. We assume that the source is lensed by an object that can be treated as a single lens plane.

Let us consider an angular coordinate system centered on a lens at redshift  $z_l$  and a source with angular position  $\beta$  at redshift  $z_s$ . According to Fermat's principle light-rays from the source follow paths that extremize the arrival-time. Let  $t(\theta, \beta)$  be the arrival-time of rays observed at an angle  $\theta$ . We can estimate this function by considering the geodesics of photons connecting the source-lens and the lens-observer planes respectively. Two effects contribute to the arrival-time, a geometrical term which accounts for the different length of the lensed paths and a gravitational term due to the Shapiro effect (for a detailed derivation e.g. see Blandford & Narayan 1986). The geometrical contribution reads as

$$t_{\text{geom}}(\theta, \beta) = \frac{1 + z_l}{2} \frac{D_l D_s}{c D_{ls}} (\theta - \beta)^2, \quad (1)$$

where  $c$  is the speed of light, while  $D_l$ ,  $D_s$  and  $D_{ls}$  are the angular diameter distances between observer and lens, observer and source, and lens and source respectively; in the following, we note  $\theta$  and  $\beta$  the norms of  $\boldsymbol{\theta}$  and  $\boldsymbol{\beta}$ . The gravitational term is given by

$$t_{\text{grav}}(\theta, \beta) = -8\pi \frac{1 + z_l}{c^3} \Psi(\theta) \quad (2)$$

<sup>3</sup> www.qgd.uzh.ch/projects/pixelens/

where  $\Psi(\boldsymbol{\theta})$  is a 2-D gravitational potential generated by the projected surface mass density on the lens plane at the angular position of the source,  $\Sigma(\boldsymbol{\theta})$ , as given by the Poisson-like equation

$$\nabla^2 \Psi(\boldsymbol{\theta}) = G\Sigma(\boldsymbol{\theta}), \quad (3)$$

where  $G$  is the Newton gravitational constant. It is useful to introduce the critical density  $\Sigma_c = \frac{c^2}{4\pi G} \frac{D_s}{D_1 D_{1s}}$ , the convergence  $\kappa = \Sigma/\Sigma_c$  and the reduced potential  $\psi = 2\Psi/(G\Sigma_c)$  to write the total arrival-time as

$$t(\boldsymbol{\theta}, \boldsymbol{\beta}) = (1 + z_l) \frac{D_1 D_s}{c D_{1s}} \left[ \frac{1}{2} (\boldsymbol{\theta} - \boldsymbol{\beta})^2 - \psi(\boldsymbol{\theta}) \right], \quad (4)$$

from which we can derive all relevant equations describing the properties of the images.

**Lens Equation:** let us assume the source to be fixed at the angular location  $\boldsymbol{\beta}$ , the arrival-time only depends on  $\boldsymbol{\theta}$  and images will form at extrema of the arrival time corresponding to  $\nabla t = 0$ . Using Eq. (4) we obtain the lens equation

$$\boldsymbol{\beta} = \boldsymbol{\theta} - \nabla \psi(\boldsymbol{\theta}). \quad (5)$$

**Magnification:** gravitational lensing deforms the images of a lensed source and since the luminosity per surface area is conserved, images can appear magnified or demagnified. The amplitude of the effect can be quantified by considering the relation between the coordinates on the source plane and the lens one. Let

$$\mathcal{A} \equiv \nabla \boldsymbol{\beta} = 1 - \nabla \nabla \psi, \quad (6)$$

be the Jacobian matrix of the angular coordinate transformation, this relation implies that a solid-angle element  $\delta\beta^2$  of the source is mapped to a solid-angle element of the image  $\delta\theta^2$  by the inverse of the determinant of  $\nabla \boldsymbol{\beta}$ . Hence, the magnification is given by

$$\mu \equiv \frac{\delta\theta^2}{\delta\beta^2} = \frac{1}{\det \mathcal{A}}. \quad (7)$$

**Time-delay:** let us consider a double-image lensed source characterized by a time-variable luminosity, the time-delay in the appearance of the luminosity variation between two images A and B is given by:

$$\begin{aligned} \Delta t_{AB} &= t(\boldsymbol{\theta}_A, \boldsymbol{\beta}) - t(\boldsymbol{\theta}_B, \boldsymbol{\beta}) = (1 + z_l) \frac{D_1 D_s}{c D_{1s}} \times \\ &\times \left[ \frac{1}{2} (\boldsymbol{\theta}_A - \boldsymbol{\beta})^2 - \psi(\boldsymbol{\theta}_A) - \frac{1}{2} (\boldsymbol{\theta}_B - \boldsymbol{\beta})^2 + \psi(\boldsymbol{\theta}_B) \right]. \end{aligned} \quad (8)$$

The position of the images, their relative flux ratios and time-delays are the main observable features of a strong lens systems.

## 2.2 Lens models

Our goal is to select a homogeneous sample of simple lens systems that can be easily observed in large sky surveys. For this reason we focus on individual galaxies which lens distant quasar sources.

### 2.2.1 Power-law density profile

The mass distribution of lens spiral and elliptical galaxies is well approximated by power-law density profiles (e.g. see Rusin 2003) for which the lens potential assume the form:

$$\psi(\boldsymbol{\theta}) = \frac{b^2}{3-n} \left( \frac{\theta}{b} \right)^{3-n}, \quad (9)$$

where  $b$  is a deflection scale. The singular isothermal sphere (SIS) model (Binney & Tremaine 1987) corresponds to  $n = 2$ , for which  $b = 4\pi D_{1s} \sigma^2 / D_s$ , where  $\sigma$  is the velocity dispersion of the galaxy. Measurements of galaxy density profiles indicates that the slope parameter  $n$  is generally close to the isothermal value, though some systems have revealed shallow profiles with  $n < 1$  (e.g. see Salucci et al. 2007). By computing the second derivative of Eq. (9) with respect to  $\theta$  we obtain the convergence:

$$\kappa(\boldsymbol{\theta}) = \frac{2-n}{2} \left( \frac{\theta}{b} \right)^{1-n}. \quad (10)$$

In the case of a double image lens with point-like images located at  $\theta_A$  and  $\theta_B$ , the deflection scale can be written as:

$$b = \left( \frac{\theta_A + \theta_B}{\theta_A^{2-n} + \theta_B^{2-n}} \right)^{\frac{1}{n-1}}, \quad (11)$$

where we have used Eq. (5). For such a system the time-delay between the two images is given by (Kochanek 2002):

$$\begin{aligned} \Delta t_{AB} &= (1 + z_l) \frac{D_1 D_s}{c D_{1s}} \times \\ &\times \left\{ (1 - \langle \kappa \rangle) \left[ \frac{1}{2} (\theta_B^2 - \theta_A^2) + \theta_A \theta_B \log \left( \frac{\theta_A}{\theta_B} \right) \right] + \right. \\ &\left. - 2 \int_{\theta_A}^{\theta_B} [\kappa(\theta) - \langle \kappa \rangle] \log \left( \frac{\theta}{\theta_B} \right) \theta d\theta \right\} \end{aligned} \quad (12)$$

where

$$\langle \kappa \rangle = \frac{2}{\theta_B^2 - \theta_A^2} \int_{\theta_A}^{\theta_B} \kappa(\theta) \theta d\theta, \quad (13)$$

is the mean surface mass density in the ring between  $\theta_A$  and  $\theta_B$ . The above formulae can be rewritten using Eq. (10):

$$\begin{aligned} \Delta t_{AB} &= (1 + z_l) \frac{D_1 D_s}{c D_{1s}} \left\{ \left[ \frac{1}{2} - \langle \kappa \rangle \frac{2-n}{3-n} \right] [\theta_B^2 - \theta_A^2] + \right. \\ &\left. + \left[ b^{n-1} \frac{\theta_A^{3-n} \theta_B^2 - \theta_B^{3-n} \theta_A^2}{\theta_B^2 - \theta_A^2} - (1 - \langle \kappa \rangle) \theta_A \theta_B \right] \ln \frac{\theta_A}{\theta_B} \right\} \end{aligned} \quad (14)$$

and

$$\langle \kappa \rangle = b^{n-1} \frac{\theta_B^{3-n} - \theta_A^{3-n}}{\theta_B^2 + \theta_A^2}, \quad (15)$$

which explicitly depend on the lens model parameters.

Similarly we can write the flux-ratios between images A and B in terms of their angular positions and the parameters of the power law potential using Eq. (7). The flux-ratio is given by

$$r_{AB} \equiv \frac{F_A}{F_B}, \quad (16)$$

where

$$\frac{1}{F_i} = \left| \left[ 1 - \left( \frac{\theta_i}{b} \right)^{1-n} \right] \left[ 1 - (2-n) \left( \frac{\theta_i}{b} \right)^{1-n} \right] \right|, \quad (17)$$

with  $i = A, B$ . This accounts only for luminosity differences between images due to lensing magnification. From Eq. (17) we can see that flux-ratio measurements can strongly constrain the lens model parameters, thus in combination with time-delays such data can reduce or break the mass-sheet degeneracy and lead to tighter bounds on cosmological parameters.

Several source of systematic errors currently limit the use of

flux-ratio measurements. In fact, these can be affected by inhomogeneous dust extinction across the angular size of the lens system, thus altering the contribution of the lens magnification encoded in the flux-ratio measurements. In principle dust effects can be taken into account through color analysis. On the other hand, rapidly varying lensing effects can be a more important source of systematic uncertainty that remains hard to model. As shown by Schild & Smith (1991) in the case of the double image lens Q0957+561 flux-ratios can vary over time. Fine variations on short time scales can be caused by microlensing of the structure of the lensed quasar, while trends over longer periods are more indicative of the mass spectrum of the lens galaxy.

Radio measurements of flux ratios are primarily affected by milli-lensing events, while in the optical both milli-lensing and micro-lensing causes flux anomalies. In the latter case flux-ratio estimates from spectroscopic measurements may alleviate the systematic effect due to micro-lensing as recently pointed out by Sluse et al. (2012).

Henceforth, it is not surprising that flux-ratios can be an effective probe of the lens mass distribution (e.g. see Goicoechea, Gil-Merino & Ullán 2005), but at the same time if unmodelled, flux anomalies introduce dominant systematic errors in the cosmological parameter inference. Overcoming these limitations requires a systematic monitoring of the lens systems phased on the lens time-delay as well as an accurate modeling of the lens inner structure. Such detailed analyses have yet to be performed and are beyond the scope of our work. Because of this cosmological constraints inferred in combination with flux-ratio measurements should be taken with a grain of salt. In Section 5.3 we will show results obtained by combining time-delays with flux ratios only for illustrative purposes.

### 2.2.2 External shear

The presence of mass perturbators outside the lens system can directly alter the lens potential and introduce uncertainties in the modeling of the lens potential. This is especially the case if a single lens galaxy is not isolated, rather is part of a group or a cluster of galaxies where an external shear field can deform the monopole potential Eq. (9). Such deformation can be modeled by adding a quadrupole term and in polar angular coordinates  $\theta = (\theta, \phi)$  this reads as

$$\psi_{\text{shear}}(\theta) = -\frac{1}{2}\gamma\theta^2 \cos 2(\phi - \phi_\gamma), \quad (18)$$

where  $\gamma$  is an amplitude parameter which measure the strength of the external shear and  $\phi_\gamma$  its direction. Observational constraints on the external shear have been mainly inferred from the study of multiple image lenses. As an example, a number of studies of individual quadruple lens systems have shown that the shear amplitude is rather large,  $\gamma \approx 0.1 - 0.3$  (Fischer, Schade & Barrientos 1998; Kneib, Cohen & Hjorth 2000). In contrast, earlier expectations were in the range  $\sim 0.02 - 0.05$  (Keeton, Kochanek & Seljak 1997). Using results from N-body simulations in combination with semi-analytic models of galaxy formation Holder & Schechter (2003) have shown that distribution of values of  $\gamma$  is nearly-Gaussian with a peak at  $\gamma \approx 0.1$  and a rapid decay for  $\gamma > 0.2$ . On the other hand Wong et al. (2011) have performed an accurate study of nine lens systems in galaxy groups and clusters which indicates that on average  $\gamma = 0.08$ , with a distribution ranging from 0.02 to 0.17.

Accounting for the effect of external shear as described by

Eq. (18) adds two parameters to the lens model. Consequently, Eq. (14)-(17) are modified by terms which explicitly depends on the external shear parameters. Such terms can be computed analytically using Eq. (18), their derivation is quite cumbersome and we leave it to Appendix A. An important aspect of the presence of external shear concerns the geometrical configuration of the images. In particular the angular separation of the images  $\Theta_{AB} = \theta_B - \theta_A$ , the asymmetry  $R_{AB} \equiv |(\theta_B - \theta_A)/(\theta_B + \theta_A)|$ , and the deviation from colinearity  $\epsilon = |\Theta_{AB} - 180|/180$  are indicators of perturbations about a monopole-like lens potential. As an example, Schneider, Kochanek & Wambsganss (2006) have shown that the time-delays have little sensitivity to the quadrupole term if the images are opposite to each other with respect to the lens position. Similarly, Oguri (2007) has shown that for image pairs with an asymmetry parameter  $R_{AB} > 0.2$  the time-delay is not significantly influenced by an external shear, a third-order external perturbation or the presence of dark matter subhalos. In contrast, for such systems the time-delay is more sensitive to the radial slope of the potential (which quantifies the deviation from isothermality), which appears to be the case especially for image pairs with a wide angular separation. This offer a first empirical criterion to select a homogeneous lens sample.

In addition to external shear, a non-spherical lens mass distribution can lead to a non-trivial angular dependence of the lens potential that contributes to the time-delay. If unmodelled this also introduce a systematic error altering the cosmological parameter inference. In the case of lenses with images lying opposite to each other the contribution from this internal shear appears only as a second order correction to the time-delay Kochanek (2002). This suggests that in general the presence of internal shear should not be neglected.

## 3 BAYESIAN STATISTICAL ANALYSIS

Our goal is to use Bayesian model selection to construct a statistically homogeneous sample of gravitational lenses from which to infer cosmological constraints using time-delays. More specifically, we aim to select lenses for which data provide strong evidence in favor of a simple power-law model description and exclude with high statistical significance the presence of external shear which might contribute to sample selection effects in single lens galaxies. Here we review the basic elements of Bayesian statistical analysis.

### 3.1 Model parameter estimation and error propagation

Let us consider a set of observations of a double image lens  $\mathbf{D}$ , consisting of the angular position of the images  $\theta_i$  ( $i = A, B$ ), the time-delay  $\Delta t_{AB}$  (and eventually flux ratio  $r_{AB}$ ). We want to constrain a lens model  $\mathcal{M}$  specified by a set of model parameters  $\alpha$ . For the time being let us assume hard priors on the cosmological parameters which determine the cosmic angular distances in Eq. (8). The first step of the data model comparison consists of inferring the best fit values of the lens model parameters as well as their uncertainties expressed in terms of ‘‘credible intervals’’. To this end we promote the model parameters to random variables and use the Bayes theorem to infer their posterior probability distribution of the parameters given the data and the model  $\mathcal{M}$ :

$$P(\alpha | \mathbf{D}, \mathcal{M}) = \frac{\tilde{\mathcal{L}}(\mathbf{D} | \alpha, \mathcal{M})P(\alpha | \mathcal{M})}{P(\mathbf{D} | \mathcal{M})}, \quad (19)$$

where  $\tilde{\mathcal{L}}(\mathbf{D} | \boldsymbol{\alpha}, \mathcal{M})$  is the likelihood function,  $P(\boldsymbol{\alpha} | \mathcal{M})$  is the prior parameter model probability and  $P(\mathbf{D} | \mathcal{M})$  is the Bayesian “evidence”. Notice that the likelihood is not a probability distribution in the parameters  $\boldsymbol{\alpha}$ , since it gives the probability of the data  $\mathbf{D}$  for a given value of the model parameters. In contrast, the evidence is the probability of the observed data within the assumed model  $\mathcal{M}$  and appears as an overall normalization constant of the posterior. Hence, for parameter estimation purposes the evidence can be neglected since we are interested in finding the maximum of the posterior and the dispersion around it. This can be done by computing the likelihood function, which for a set of independent data reads as:

$$\tilde{\mathcal{L}}(\mathbf{D} | \boldsymbol{\alpha}, \mathcal{M}) \equiv e^{-\frac{\chi^2}{2}} = \exp \left\{ - \sum_i \frac{[D_i - D_{\text{th}}^i(\boldsymbol{\alpha})]^2}{2\sigma_i^2} \right\}, \quad (20)$$

where  $\sigma_i$  are the observational uncertainties and  $D_{\text{th}}^i(\boldsymbol{\alpha})$  are the model predictions. However, notice that in our case, the position of the images,  $\theta_A$  and  $\theta_B$ , play the role of independent variables in  $\Delta t_{\text{AB}}$  and  $r_{\text{AB}}$  respectively. Since, the measured angles are known up to observational errors, it is important to propagate the angular uncertainties as well. This can be consistently done in the Bayesian framework. For a detailed discussion on the subject we refer to the exhaustive article by D’Agostini (D’Agostini 2005).

Let assume that the observed image positions,  $\theta_A$  and  $\theta_B$ , are determined with Gaussian uncertainties  $\sigma_A$  and  $\sigma_B$  respectively. Let us indicate with  $\Theta_A$  and  $\Theta_B$  the true location of the images. Then, we can propagate the uncertainty on the independent variables by marginalizing the likelihood over the angular error distribution. Assuming Gaussian errors this gives (for conciseness we drop the dependence on  $\mathcal{M}$ ):

$$\mathcal{L}(\mathbf{D} | \boldsymbol{\alpha}) = \iint f(\Theta_A, \Theta_B) \tilde{\mathcal{L}}(\mathbf{D} | \Theta_A, \Theta_B, \boldsymbol{\alpha}) d\Theta_A d\Theta_B, \quad (21)$$

with

$$f(\Theta_A, \Theta_B) = \exp \left\{ - \sum_{A,B} \frac{(\theta_i - \Theta_i)^2}{2\sigma_i^2} \right\}, \quad (22)$$

where in the integrand we have explicitated the dependence of the likelihood  $\tilde{\mathcal{L}}$  on the position of the images. If the angles are precisely measured, then Eq. (22) tends to a  $\delta$ -Dirac and we recover the standard likelihood expression Eq. (20).

### 3.2 Bayesian model selection

Parameter estimation only provides us with information on the quality of fit of a given model against the data. How do we choose between competing models characterized by different model parameters? Preference solely based on the goodness-of-fit as measured by the  $\chi^2$  for the best fitting model parameter values leaves us with partial information which is not consistently quantifiable in a probabilistic manner. Even then, how do we discount for the level of predictiveness of different models? More precisely, how do we decide whether data justify the choice of a more complex model  $\mathcal{M}_1$  over one with a smaller number of free parameters  $\mathcal{M}_0$ , while accounting for the extended prior parameter space of  $\mathcal{M}_1$ ? As stressed in Liddle et al. (2007), such a question is related to the predictiveness of models rather than ‘simplicity/complexity’, since the former is not necessarily related to the number of free parameters. Parameter estimation does not address these questions, which require a further step already built in the Bayesian approach.

Central object of the Bayesian model selection is the evidence,

$$P(\mathbf{D} | \mathcal{M}) = \int d\boldsymbol{\alpha} \mathcal{L}(\mathbf{D} | \boldsymbol{\alpha}, \mathcal{M}) P(\boldsymbol{\alpha} | \mathcal{M}), \quad (23)$$

which gives the probability of the data given the model  $\mathcal{M}$ . Using the Bayes theorem we then have the probability of the model  $\mathcal{M}$  given the data,

$$P(\mathcal{M} | \mathbf{D}) \propto P(\mathbf{D} | \mathcal{M}) P(\mathcal{M}), \quad (24)$$

where  $P(\mathcal{M})$  is the prior belief on the model. Thus, given two competing models,  $\mathcal{M}_0$  and  $\mathcal{M}_1$ , we can base our preference on the ratio of the model probabilities given the same set of data

$$\frac{P(\mathcal{M}_0 | \mathbf{D})}{P(\mathcal{M}_1 | \mathbf{D})} = \frac{P(\mathbf{D} | \mathcal{M}_0) P(\mathcal{M}_0)}{P(\mathbf{D} | \mathcal{M}_1) P(\mathcal{M}_1)}, \quad (25)$$

where the ratio

$$B_{01} = \frac{P(\mathbf{D} | \mathcal{M}_0)}{P(\mathbf{D} | \mathcal{M}_1)}, \quad (26)$$

is the so called “Bayes factor” of  $\mathcal{M}_0$  to  $\mathcal{M}_1$ . Supposing we have the same prior belief on the two models, then the Bayes factor gives us an estimate of the ratio of the model probabilities given the data. Since the evidence sets up a tension between the quality of fit of a given model and its prior predictiveness, then the Bayes factor accounts for the different size of the prior parameter space of the competing models.

Bayes factors provide us with a self-consistent probabilistic measure to select a sample of lenses for which the observational data provide strong evidence in favor of a given model description. For instance, a simple lens model is the isothermal sphere which has no free parameters,  $\mathcal{M}_0 = \{n = 2\}$ . Using the Bayes factor we can compare it to a more complex description such as the power-law model with one free parameter  $\mathcal{M}_1 = \{n\}$ . In such a case we say that  $\mathcal{M}_0$  is nested in  $\mathcal{M}_1$ . Similarly, we can compare the power-law model with one free parameter  $\mathcal{M}_0 = \{n\}$  to the case in which a shear field is included with two additional free parameters  $\mathcal{M}_1 = \{n, \gamma, \phi_\gamma\}$ . The additional presence of internal shear can be included in a third nested model  $\mathcal{M}_2$  and confronted against  $\mathcal{M}_0$  and  $\mathcal{M}_1$ . For simplicity, we limit our current analysis to the latter models only.

In order to assess the strength of evidence in favor of a model  $\mathcal{M}_0$ , against a more complex one,  $\mathcal{M}_1$ , we use the Jeffreys scale (Jeffreys 1961) as reported in Trotta (2007). To be as conservative as possible, we select lenses for which  $\ln B_{01} > 5$  and exclude those which provide strong evidence in favor of external shear, i.e.  $\ln B_{10} > 5$ . We also exclude lenses for which we consider the model comparison to be inconclusive  $-5 < \ln B_{01} < 5$ . Notice that  $\ln B_{01} = 5$  corresponds to odds of 1 in about 150 in favor of  $\mathcal{M}_0$ . The arrival of new data update these odds, further improving our knowledge of the lens system.

## 4 TESTING BAYESIAN MODEL SELECTION

In this section we perform a detailed analysis on a synthetic lens catalog to quantify the level of bias on the value of  $H_0$  inferred from a Bayes factor selected subsample of simulated lenses. To be as conservative as possible we consider lenses in the presence of external shear. This allows us to test to which extent Bayes factors can select those systems for which a simple power-law potential is sufficient to describe the simulated data and consequently evaluate the systematic bias on the inferred value of  $H_0$ .

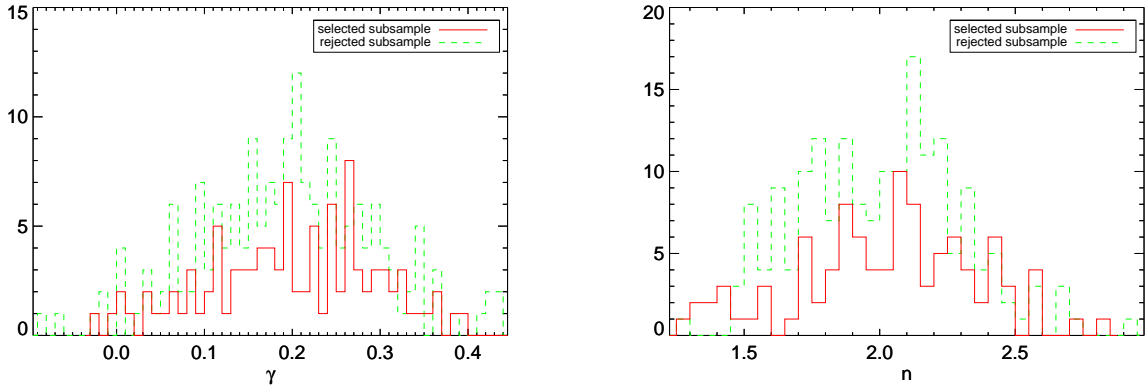


**Figure 1.** Histogram showing the distribution of simulated values of  $\gamma$  (left panel) and  $n$  (right panel) for the selected subsample  $\mathcal{S}_0$  (solid red line) and the remaining dataset  $\mathcal{S}_1$  (green dash line).

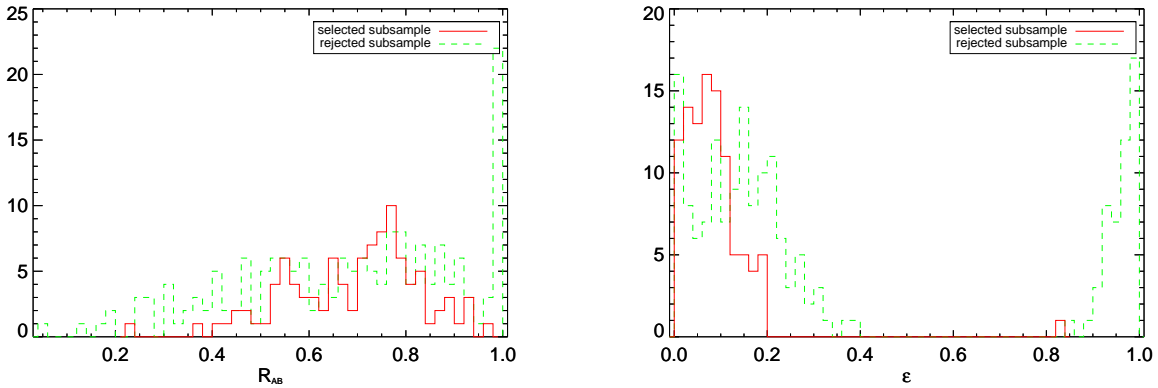


**Figure 2.** Histogram showing the distribution of values of  $R_{AB}$  (left panel) and  $\epsilon$  (right panel) for the selected subsample  $\mathcal{S}_0$  (solid red line) and the rejected dataset  $\mathcal{S}_1$  (green dash line).

#### 4.1 Synthetic Lens Catalogue

We assume a flat  $\Lambda$ CDM model with  $\Omega_m = 0.3$  and a reduced Hubble constant  $h = 0.72$ . Using the publicly available software GRAVLENS (Keeton 2011) we generate a sample of 500 gravitational lenses at  $z_l = 0.5$  with sources at  $z_s = 1.8$ . A more realistic simulation would be to distribute lenses and sources over a range of redshifts compatible with observations. However, this choice is not relevant to the purpose of this analysis and for simplicity we assume them to be at the same redshifts.

The synthetic catalogue is built by Monte Carlo generating a distribution of values of  $n$  and  $\gamma$  drawn from Gaussian distributions with  $n \sim \mathcal{N}(2, 0.3)$  and  $\gamma \sim \mathcal{N}(0.2, 0.1)$  consistently with current observational constraints discussed in Section 2.2. The position of sources is drawn from a uniform distribution in a cartesian angular map with coordinates  $-1 < x, y < 1$ . For simplicity we fix  $b = 1$ . For each simulated lens, GRAVLENS computes the number, position and time-delay of the images. Out of 500 simulated lenses only 312 have more than one image. In particular, 280 lenses with two or three images (double lenses) and 32 with four or five images (quad lenses). For simplicity we limit our analysis to the double lens subsample, since quad lenses require an accurate modeling of the lens angular structure which is essential to explain the formation of four images. We assume a 10% error on the time-delay, rather higher

than the current mean error, and neglect angular errors on the image positions.

#### 4.2 Model Selection and Systematic Bias

Using the data in the reduced catalogue, we compute the likelihood function  $\tilde{\mathcal{L}}$  over the prior lens parameter space of a simple power-law model  $\mathcal{M}_0 = \{n\}$  and one including external shear  $\mathcal{M}_1 = \{n, \gamma, \phi_\gamma\}$  respectively. We assume uniform priors with  $n \in (1, 3)$  and  $\gamma \in (0, 0.2)$ . Then, we perform a numerical integration to evaluate the bayesian evidence of each model and compute the Bayes factor, assuming a fixed cosmology with  $h = 0.7$ . Given the limited number of parameters we do not perform a Monte Carlo sampling of the likelihood, rather we compute it on a fine multi-dimensional grid.

We select all lenses with  $\ln B_{01} > 2.5$ . This gives us a subsample,  $\mathcal{S}_0$ , consisting of 111 lenses for which image astrometry and time-delay provide strong evidence in favor of a simple power-law model description. We define the remaining lenses as the subsample  $\mathcal{S}_1$ .

In Fig. 1 is shown the distribution of value of  $\gamma$  (left panel) and  $n$  (right panel) for  $\mathcal{S}_0$  (solid red line) and the remaining dataset  $\mathcal{S}_1$  (green dash line). As we can see the two subsamples cover the same range of values, thus indicating that Bayes factors are not sys-

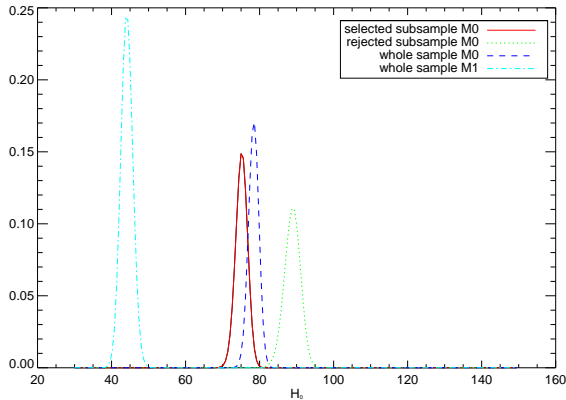


**Figure 3.** Marginalized likelihoods on  $H_0$  from the analysis of  $\mathcal{S}_0$  (solid red line),  $\mathcal{S}_1$  (green dot line) and the entire sample  $\mathcal{S}_0 + \mathcal{S}_1$  (dark blue dash line), all with model  $\mathcal{M}_0$ . The dash-dotted light-blue line is obtained by analysing the entire sample with model  $\mathcal{M}_1$ . This model is underconstrained by time-delay and astrometry data only, hence it is not surprising that due to the unbounded parameter degeneracies the inferred value of  $H_0$  strongly differs from the fiducial one.

tematically selecting lenses with particular slope profiles or small external shear amplitude. This might seem at odd with using the selected subsample  $\mathcal{S}_0$  to perform an unbiased parameter estimation using the simpler model  $\mathcal{M}_0$ . However, as extensively discussed in related literature (e.g. see Mukherjee et al. 2006), what the Bayes factors do is to put a tension between the capacity of the extended model  $\mathcal{M}_1$  to better fit the data and its larger prior parameter volume relative to the simpler model. Hence, even though the selected sample of lenses has non-vanishing shear, the data (image astrometry and time-delay) do not justify the more complex model because the gain in fitting with external shear parameters is minimal compared to the size of the enlarged prior parameter space. The Bayes factors simply tell us that the simpler model  $\mathcal{M}_0$  has to be preferred as it does a better job at describing the data with a smaller prior parameter space. By construction all simulated lenses have external shear and not surprising more than half of them are indeed discarded by the Bayes factor either as inconclusive or as favoring model  $\mathcal{M}_1$ .

In Fig. 2 we plot the histogram of the values of  $R_{AB}$  and  $\epsilon$  for  $\mathcal{S}_0$  and  $\mathcal{S}_1$  respectively. We may notice that in  $\mathcal{S}_0$  the distribution of values of  $R_{AB}$  has a smaller scatter than for  $\mathcal{S}_1$  with  $R_{AB} > 0.35$ . Similarly the distribution of values of  $\epsilon$  for the subsample  $\mathcal{S}_0$  is narrower than  $\mathcal{S}_1$  and limited to values with  $\epsilon < 0.2$ . This clearly indicate that the Bayes factor analysis has selected lenses for which the angular configuration of the images is characteristics of double lens system whose astrometry and time-delays are less sensitive to external shear effect (e.g. see Oguri 2007), hence successfully described by a simple model. Thus, the Bayes factors automatically performs an empirical model selection based on the structural properties of the lens systems.

We are now in a position to quantify the bias on the inferred value of  $H_0$  from the selected lens subsample. Assuming model  $\mathcal{M}_0$  we run a likelihood analysis on  $\mathcal{S}_0$ ,  $\mathcal{S}_1$  and their combination  $\mathcal{S}_0 + \mathcal{S}_1$ . The marginalized likelihoods on  $H_0$  are shown in Fig. 3. From  $\mathcal{S}_0$  we find  $H_0 = 75.94^{+1.5}_{-1.4} \text{ km s}^{-1} \text{ Mpc}^{-1}$ , quite remarkably this recovers the fiducial value  $H_0 = 72 \text{ km s}^{-1} \text{ Mpc}^{-1}$  to within  $3\sigma$  statistical uncertainty of the best fit value, thus indicating a systematic bias of  $\sim 5\%$ . In contrast, the analysis of  $\mathcal{S}_1$  gives a highly biased value with  $H_0 = 90.45^{+2.4}_{-2.1} \text{ km s}^{-1} \text{ Mpc}^{-1}$ , while

the combined analysis gives  $H_0 = 78.39 \pm 1.5 \text{ km s}^{-1} \text{ Mpc}^{-1}$ . In principle, the residual  $\sim 5\%$  systematic bias in  $\mathcal{S}_0$  can be reduced or possibly removed using additional lens measurements. Here, we have limited to use time-delay and astrometry data only to perform a proof of concept assuming simple lens toy models. However, in a real setup, the availability of the stellar kinematic measurements of the lens galaxy as well as high resolution imaging of the Einstein ring may provide additional constraints on the lens mass distribution, thus reducing the internal lens model parameter degeneracy, which can lead to a more accurate lens model selection and consequently less biased results. In fact, the former provides an independent estimate of the lens mass at a radius different from that of the Einstein ring (Treu et al. 2006), while the thickness of the Einstein ring is sensitive probe of the density profiles (e.g. see Suyu et al. 2009). This is to say that the residual systematic bias we have found from the analysis of the simulated lenses is not inevitable in strong lens cosmography.

One may wonder whether analysing the entire dataset using model  $\mathcal{M}_1$  may lead to less biased results given that the data have been generated using such a model. However, we should remind that model  $\mathcal{M}_1$  is underconstrained using double lenses. This can introduce very large parameter degeneracies and eventually strongly bias the cosmological parameter inference. To this purpose we have run a likelihood analysis of the whole sample  $\mathcal{S}_0 + \mathcal{S}_1$  assuming model  $\mathcal{M}_1$ . The marginalized likelihood on  $H_0$  is plotted in Fig. 3 (dash-dotted light-blue line) from which we obtain  $H_0 = 44 \pm 1.5 \text{ km s}^{-1} \text{ Mpc}^{-1}$ . This shows how subtle the parameter inference can be. In a real dataset we will not know a priori whether external shear is indeed present or not. Thus, given a set of data which we aim to use to extract cosmological parameter information we are better guided by Bayesian model selection than blindly adding parameters to model the complexity behind the data. However, as already stressed above we should not despair since additional constraints from independent mass proxies may help reduce or break internal model parameter degeneracies and consequently the robustness of the lens model selection.

## 5 APPLICATION TO REAL LENS DATA

### 5.1 Data sample

Gravitational time-delays have been measured in 21 strong lens systems. Out of this sample we only consider double image lenses in which a far distant quasar is lensed into two images by a foreground galaxy. This reduces our initial dataset to 12 lenses, whose characteristics are quoted in Table 1. The object responsible for the lensing has been unambiguously detected in all listed lenses. However, current observations do not provide clear indications whether the lensing galaxies are part of a group/cluster or whether perturbators are present along the line of sight. Thus, the presence of external shear cannot be a priori excluded, potentially leading to bias selection effects.

For each lens in the sample we compute the asymmetry  $R_{AB}$ , the angular separation  $\Theta_{AB}$  and the deviation from colinearity  $\epsilon$  as indicators of perturbations about a monopole-like lens potential. These are also given in Table 1, while in Table B1 in Appendix B we report the astrometry.

**Table 1.** Double-image lenses.  $z_l$  and  $z_s$  are the lens and source redshift respectively,  $\theta_i$  are the angular position of the images relative to the lens position in arcsec,  $\Delta t$  is the time-delay (in days) and  $F_i/F_j$  the flux-ratios. Observational uncertainties are  $1\sigma$  errors. We also quote the derived values of the asymmetry  $R_{AB}$ , angular separation  $\Theta_{AB}$  and deviation from colinearity  $\epsilon$ .

Lens	pair (i,j)	$z_l$	$z_s$	$\theta_i$ (")	$\theta_j$ (")	$\Delta t = t_i - t_j$	$\frac{F_i}{F_j}$	$R_{AB}$	$\Theta_{AB}$	$\epsilon$
B0218+357 <sup>a</sup>	BA	0.685	0.944	$0.057 \pm 0.004$	$0.280 \pm 0.008$	$+10.5 \pm 0.2$	$0.26 \pm 0.005$	0.66	205.6	0.14
B1600+434 <sup>b</sup>	AB	0.414	1.589	$1.14 \pm 0.075$	$0.25 \pm 0.074$	$-51.0 \pm 2.0$	$1.75 \pm 0.34$	0.45	200.2	0.11
FBQ 0951+2635 <sup>c</sup>	AB	0.260	1.246	$0.886 \pm 0.004$	$0.228 \pm 0.008$	$-16.0 \pm 2.0$	$3.15 \pm 0.05$	0.59	201.2	0.12
HE 1104-1805 <sup>d</sup>	AB	0.729	2.319	$1.099 \pm 0.004$	$2.095 \pm 0.008$	$+152.2 \pm 3.0$	$2.84 \pm 0.06$	0.32	175.9	0.02
HE 2149-2745 <sup>e</sup>	AB	0.603	2.033	$1.354 \pm 0.008$	$0.344 \pm 0.012$	$-103.0 \pm 12.0$	$4.0 \pm 0.5$	0.59	178.9	0.006
PKS 1830-211 <sup>f</sup>	AB	0.89	2.507	$0.67 \pm 0.08$	$0.32 \pm 0.08$	$-26 \pm 5$	$1.03 \pm 0.02$	0.36	199.5	0.11
Q0142-100 <sup>g</sup>	AB	0.49	2.719	$1.855 \pm 0.002$	$0.383 \pm 0.005$	$-89 \pm 11$	$6.3 \pm 0.1$	0.66	167.8	0.07
Q0957+561 <sup>h</sup>	AB	0.36	1.413	$5.220 \pm 0.006$	$1.036 \pm 0.11$	$-417.09 \pm 0.07$	$1.35 \pm 0.04$	0.67	154.5	0.14
SBS 0909+532 <sup>i</sup>	AB	0.830	1.377	$0.415 \pm 0.126$	$0.756 \pm 0.152$	$+45.0 \pm 5.5$	$0.32 \pm 0.03$	0.29	220.3	0.22
SBS 1520+530 <sup>j</sup>	AB	0.717	1.855	$1.207 \pm 0.004$	$0.386 \pm 0.008$	$-130.0 \pm 3.0$	$2.9 \pm 0.4$	0.52	202.6	0.13
SDSS J1206+4332 <sup>k</sup>	AB	0.748	1.789	$1.870 \pm 0.088$	$1.278 \pm 0.097$	$-116 \pm 5$	$0.74 \pm 0.2$	0.19	132.9	0.26
SDSS J1650+4251 <sup>l</sup>	AB	0.577	1.547	$0.872 \pm 0.027$	$0.357 \pm 0.042$	$-49.5 \pm 1.9$	$6.2 \pm 0.31$	0.42	145.8	0.19

<sup>a</sup> Image positions from Lehár et al. (2000) computed relative to the lens center as measured by York et al. (2005); lens and source redshifts from Browne et al. (1993) and Cohen et al. (2003) respectively, time-delay from Biggs et al. (1999) and flux ratio from Wucknitz, Biggs & Browne (2004).

<sup>b</sup> Image positions and redshifts from Koopmans, de Bruyn & Jackson (1998), time-delay from Burud et al. (2000), flux-ratio from Dai & Kochanek (2005).

<sup>c</sup> Image positions and redshifts as listed in Kochanek et al. (2008), time-delay from Jakobsson et al. (2005), flux-ratio from Shalyapin et al. (2009).

<sup>d</sup> Image positions and redshifts from Lehár et al. (2000), time-delay and flux-ratio from Poindexter et al. (2007).

<sup>e</sup> Image positions and redshifts as listed in Kochanek et al. (2008), time-delay and flux-ratio from Burud et al. (2002a).

<sup>f</sup> Image positions and redshifts from Meylan et al. (2005), time-delay from Lovell et al. (1998), flux-ratio from Courbin et al. (1998).

<sup>g</sup> Image positions and redshifts as listed in Kochanek et al. (2008), time-delay and flux-ratio from Koptelova et al (2012).

<sup>h</sup> Image positions and redshifts as listed in Kochanek et al. (2008), time-delay from Colley et al. (2003), flux-ratio from Haarsma et al. (1999).

<sup>i</sup> Image positions and redshifts as listed in Kochanek et al. (2008), time-delay from Ullán et al. (2006), flux-ratio from Dai & Kochanek (2009).

<sup>j</sup> Image positions and redshifts as listed in Kochanek et al. (2008), time-delay from Burud et al. (2002b), flux-ratio from Auger et al. (2008).

<sup>k</sup> Image positions and redshifts as listed in Oguri et al (2005), time-delay and flux-ratio from Paraficz, Hjorth & Eliasdóttir (2009).

<sup>l</sup> Image positions and redshifts as listed in Kochanek et al. (2008), time-delay and flux-ratio from Vuissoz et al. (2007).

## 5.2 Model parameter priors

We want to test whether the data listed in Table 1 provide strong evidence for or against a simple power-law model,  $\mathcal{M}_0 = \{n\}$ , or one which includes external shear,  $\mathcal{M}_1 = \{n, \gamma, \phi_\gamma\}$ . Uninformative data cause the Bayes factors to depend on the size of the assumed prior parameter space. To test for such dependence we distinguish two different sets of priors for each lens model parameter.

To be as conservative as possible we assume a uniform “large prior” on the radial slope of the potential,  $n \in (0, 3)$  and a uniform “small prior” corresponding to  $n \in (1, 3)$ . The former includes shallow galaxy profiles ( $n < 1$ ) such as those found in e.g. Salucci et al. (2007), while the latter is limited to the cuspy profiles, including the isothermal sphere, which are typical of Cold Dark Matter halos. Similarly, we assume flat priors on  $\gamma$  and consider two prior intervals,  $\gamma \in (0, 0.1)$  and  $\gamma \in (0, 0.2)$ , while the external shear orientation angle is assumed  $\phi_\gamma \in (0, \pi)$ .

In the evaluation of the Bayes factors we consider a flat concordance  $\Lambda$ CDM model and assume for simplicity a value compatible with WMAP-7yr (Larson et al. 2011) on the matter density,  $\Omega_m = 0.27$ . In order to test the dependence of the Bayes factors on the value of the Hubble constant we assume three prior values:  $H_0 = 65, 70.2$  and  $75 \text{ km s}^{-1} \text{ Mpc}^{-1}$  respectively.

## 5.3 Bayes factor analysis

The results of the numerical computation of the Bayes factors obtained from the analysis of time-delays and image astrometry are

summarized in Fig. 4, while in Fig. 5 we show the results obtained including flux-ratio measurements. For each lens in the sample we mark the value of  $\log_{10} B_{01}$  under different lens model parameter priors and for values of the Hubble constant  $H_0 = 65$  (left panel),  $70.2$  (middle panel) and  $75 \text{ km s}^{-1} \text{ Mpc}^{-1}$  (right panel) respectively. The hatched areas correspond to values of the Bayes factors for which the data provide strong evidence in favor of the simple power-law description ( $\ln B_{01} > 5$ ), the presence of external shear ( $\ln B_{10} > 5$ ). We assume the Bayes model comparison to be inconclusive in the region  $-5 < \ln B_{01} < 5$  which is a very conservative cut.

Let us focus on Fig. 4. First we can see that Bayes factors show no variation for the large and small priors on  $n$ , except for Q0957+561. On the other hand, most lenses exhibit prior dependence on  $\gamma$ , which can vary in strength with the cosmology. FBQ 0951+2635, HE 2149-2745 and Q0957+561 are the only ones for which the prior on  $\gamma$  seems to have no influence whatsoever. We may also notice a weak dependence of the Bayes factors on the value of  $h$ . In particular, B1600+434 and SDSS J1650+4251 have Bayes factor which are clearly above our conservative cut for  $h = 0.702$  and  $h = 0.75$ , while these shift in the upper bound on the inconclusive interval for  $h = 0.65$ . However, since the value of  $B_{01}$  is still rather high, these lenses would pass a slightly less conservative cut even in the worst case scenario of  $h = 0.65$ .

All lenses except HE 1104-1805 and Q0957+561 have Bayes factors favoring  $\mathcal{M}_0$ , though they may lie in the inconclusive area. Q0957+561 is the only lens clearly favoring model  $\mathcal{M}_1$  in some case. One final remark concerns SBS 1520+530. Our analysis in-



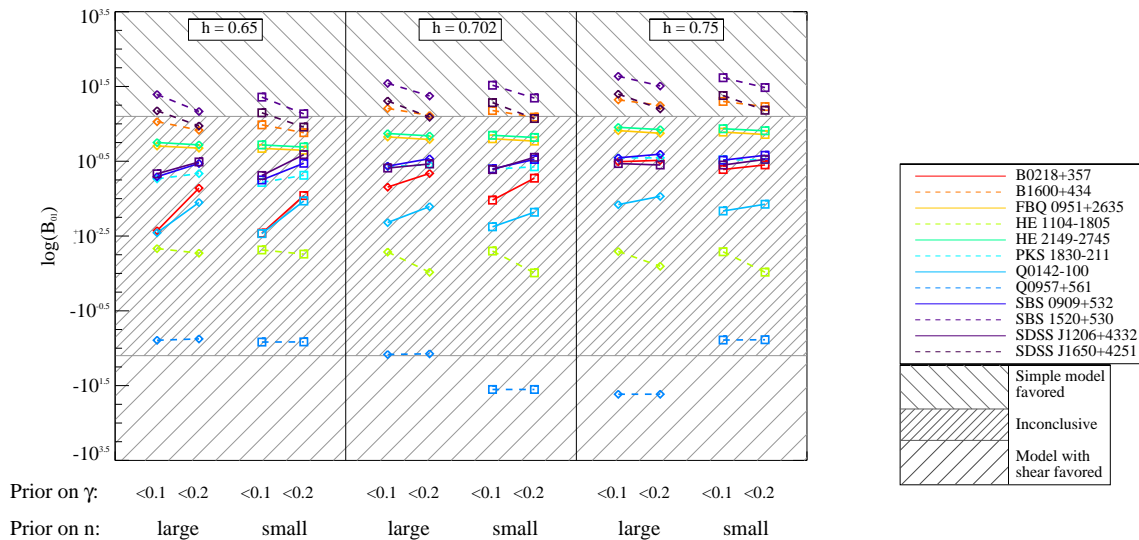


**Figure 4.** Bayes factors for the sample of lenses listed in Table 1 and obtained from the analysis of the image positions and time-delays for different lens model parameter priors and assuming a hard prior on the reduced Hubble parameter with  $h = 0.65$  (left panel),  $h = 0.702$  (middle panel) and  $h = 0.75$  (right panel).

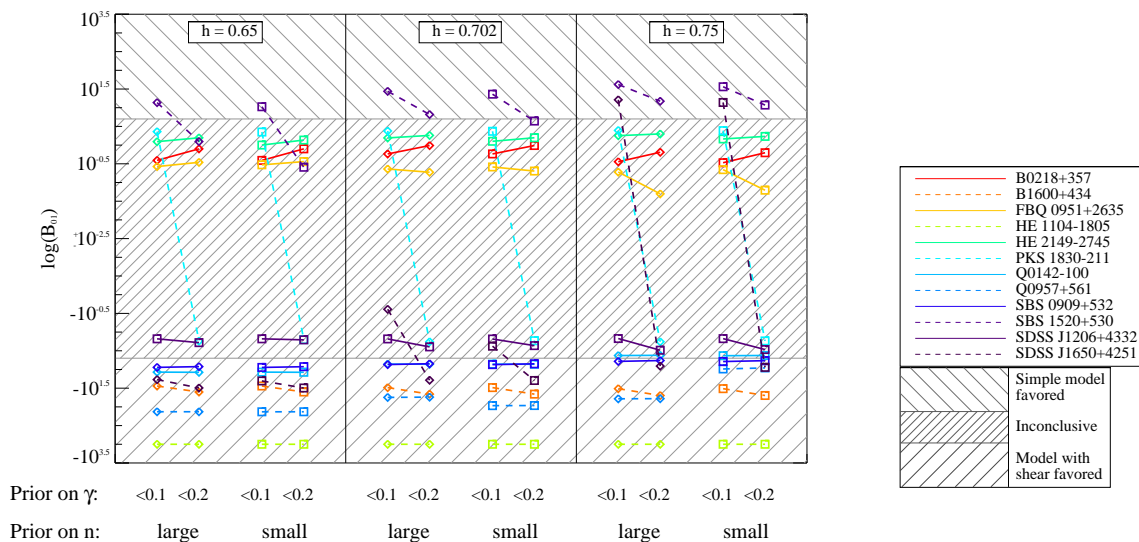


**Figure 5.** As in Figure 4 including information from flux-ratio measurements.

indicates that the image position and the time-delay of this lens strongly favor a simple power-law lens model without external shear. This is not in contrast with observations of the lens properties by Auger et al. (2008) who have shown the presence of galaxy groups at nearby redshifts on the lens line of sight. It is plausible that mass potential is centered on the lens (as suggested by the galaxy-groups position relative to the lens) thus implying a negligible quadrupole contribution. Hence, as discussed in section 4 the extra parameters from modeling the external shear may provide a minimal gain in fitting the data and in such a case the Bayes factor favours the simpler model description. Furthermore, Auger et al. (2008) find that the system can be well fitted by a nearly isothermal density profile.

In Fig. 5 we plot the Bayes factors obtained from time-delays and flux-ratio measurements. As we can see including flux-ratios shifts the Bayes factors of several lens systems in the range which

strongly favor the presence of external shear. However, it is possible that the extra parameters of model  $\mathcal{M}_1$  fit unmodeled systematics affecting the flux-ratios rather than the effects of an external shear field. As already mentioned in Section 2.2, current observations already indicate that dust extinction as well as microlensing and substructure alter the flux-ratios. Since we are far from being able to quantitatively account for such contaminations, it is premature to infer any conclusion based on these data.

In the light of the analysis of Bayes factors inferred from position of the lens images and time-delays we select B1600+434, SBS 1520+530 and SDSS J1650+4251 out of the initial lens sample. These are the only lenses which pass our selection criterion independently of the model parameter priors with the power-law model strongly favored over that including external shear with odds of more than 150 to 1. In the next Section we will present the constraints on  $H_0$  obtained from the likelihood analysis of these lenses.

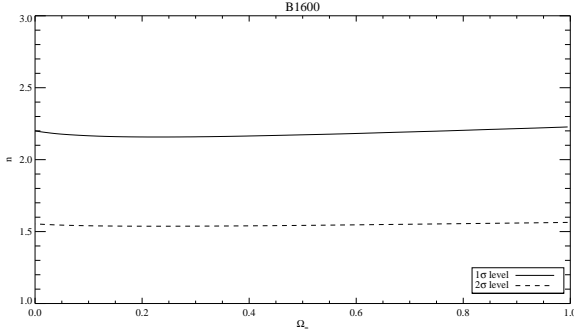


**Figure 6.** Marginalized 1 and  $2\sigma$  contours in the  $\Omega_m - n$  plane without WMAP prior for B1600-434.

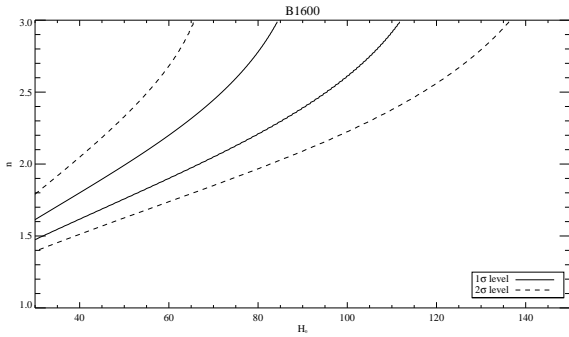


**Figure 7.** As in Fig. 6 for the  $H_0 - n$  plane without WMAP prior.

## 6 COSMOLOGICAL PARAMETER INFERENCE

Using the image positions and time-delays of B1600+434, SBS 1520+530 and SDSS J1650+4251, we perform a likelihood analysis to infer constraints on  $H_0$  after marginalizing over the angular errors of the image locations, the slope of the power-law model of each lens  $n_i$  and the matter density  $\Omega_m$ . We assume flat priors on  $1 < n < 3$  and  $30 < H_0 [\text{km s}^{-1} \text{Mpc}^{-1}] < 150$ . For each lens we compute the likelihood function  $\mathcal{L}(n_i, \Omega_m, H_0)$  as given by Eq. (21). We illustrate the parameter degeneracies for B1600+434, in Fig. 6 and Fig. 7 we plot the 1 and  $2\sigma$  marginalized contours in the planes  $\Omega_m - n$  and  $H_0 - n$  respectively. We can see that there is no correlation between  $n$  and  $\Omega_m$  for such dataset, while a more pronounced degeneracy is present between  $n$  and  $H_0$ , as was already pointed in Suyu (2012). Introducing a prior on  $\Omega_m$  does not change the likelihood contour significantly, as there is little degeneracy between  $\Omega_m$  and either  $n$  or  $H_0$ .

In Fig. 8 we plot the 1-dimensional marginalized likelihoods in the prior interval of  $n$  for each of the lenses obtained assuming a Gaussian prior on  $\Omega_m = 0.266 \pm 0.029$  consistent with WMAP7-yrs results (Larson et al. 2011). We can see that data can only provide a lower limit on the value of the slope of the lens potential,  $n \gtrsim 1.5$ . Similarly, in Fig. 9 we plot the marginalized likelihoods of  $H_0$  for each lens. We may notice that the likelihoods peak around nearly the same value of  $H_0$  and have a large dispersion around the maximum value.

The combined constraints on  $H_0$  are inferred by computing the total likelihood sample:

$$\mathcal{L}(\Omega_m, H_0) = \prod_i \int \mathcal{L}(n_i, \Omega_m, H_0) P(n_i) dn_i, \quad (27)$$

where the sum is over the likelihood of each lens weighted by  $P(n_i)$  the uniform prior in the interval  $1 < n_i < 3$ . Hence, we

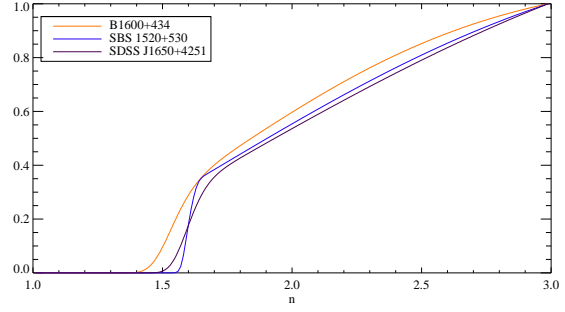


**Figure 8.**  $\mathcal{L}(n | \Omega_m, H_0) / \mathcal{L}_{\max}$  for each of the selected lenses.

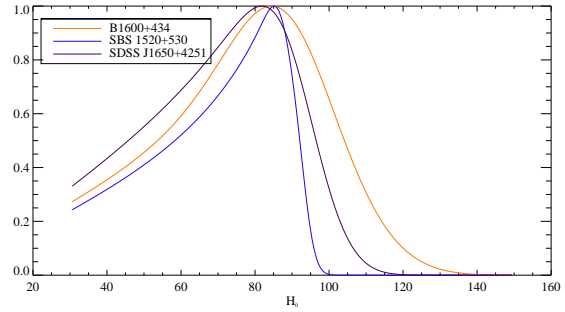


**Figure 9.**  $\mathcal{L}(H_0 | \Omega_m, n) / \mathcal{L}_{\max}$  for each of the selected lenses.

do not assume a hard prior on  $n$  at the best-fit value of each lens, rather we impose the model and propagate its parameter uncertainties by marginalising the likelihood over them. In Fig. 10 we plot the 1 and  $2\sigma$  contours in the  $\Omega_m - H_0$  plane (left panel) and the 1-dimensional marginalized likelihood for  $H_0$  (right panel) with and without WMAP7-yrs prior. As we can see, time-delays are mostly insensitive to  $\Omega_m$ . The average and standard deviation values are  $H_0 = 76_{-5}^{+15} \text{ km s}^{-1} \text{Mpc}^{-1}$  and  $H_0 = 78_{-5}^{+15} \text{ km s}^{-1} \text{Mpc}^{-1}$  without and with WMAP7-yr prior respectively. Notice that the marginalized likelihood is non-Gaussian and strongly skewed towards small values of  $H_0$ . Thus, the average values differ the maximum ones which are at  $H_0 = 85 \text{ km s}^{-1} \text{Mpc}^{-1}$  and  $H_0 = 88 \text{ km s}^{-1} \text{Mpc}^{-1}$  without and with WMAP7-yr prior respectively.

It is worth highlighting that, while on the observational sample, about a quarter (three out of twelve) of the lenses are selected through our analysis, in the simulated sample this ratio is higher than a third (111 out of 280), which seems to indicate that observational samples are more contaminated than our simulated sample, leading to possibly higher bias if the whole sample is used to measure  $H_0$ .

## 7 CONCLUSIONS

In this study we have used Bayesian model selection techniques to determine the lens mass model which given the data has the highest probability to describe a strong gravitational lens system. Rather than modeling a lens in all its complexity, our goal is to focus on selecting a model whose parameters can significantly influence the time-delay such as to infer unbiased cosmological constraints when averaging individual mass model parameter uncertainties on a homogeneous lens sample. To this end we have focused on double lenses and used Bayes factor statistics to select a sample of lenses that can be described by a power-law model without external shear.

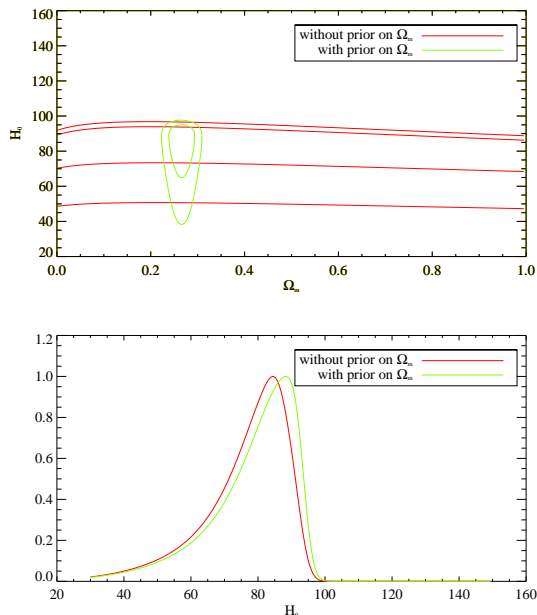


**Figure 10.** Top panel: 1 and  $2\sigma$  contours  $\Omega_m - H_0$  plane from the combined analysis of the selected lens sample. Bottom panel:  $\mathcal{L}(H_0)/\mathcal{L}_{\max}$  for the same sample.

We have tested this approach on a simulated sample of 500 lenses. The likelihood analysis of the selected subsample assuming no external shear recovers the fiducial value of the Hubble constant with  $3\sigma$  statistical uncertainty, thus a systematic selection bias is no greater than  $\sim 5\%$ . On the other hand, since the more complex model including external shear parameter is underconstrained using double lenses, the likelihood analysis result in strongly biased results due to the marginalized effects of large lens model parameter degeneracies. Therefore, a given set of data should not be brute force analysed assuming the model capable of accounting for the maximal complexity. Rather, performing a Bayes factor analysis may provide a more effective guide to data model selection.

The application to a sample of observed lenses indicates that out of the initial dataset, nine have Bayes factors favoring a simple power-law lens model, though six of them lies in the “inconclusive” interval and do not pass our conservative cut. These are B0218+357, FBQ 0951+2635, HE 2149-2745, PKS 1830-211, Q0142-100, and SBS 0909+532. It is possible that more accurate time-delay measurements will update their Bayes factor value and give us a better knowledge of the appropriate lens model description. We have performed the same analysis including information from lens flux-ratio measurements. In such a case, the Bayes factors indicate that external shear must be taken into account for most of the lenses. However, several source of astrophysical systematic errors may affect the flux-ratios such as dust extinction and microlensing events that do not reflect the lensing magnification caused by the lens mass distribution responsible for the images and time-delays. Indeed, uncontaminated flux-ratios will provide interesting additional constraint on the lens model. Nevertheless, it is worth reminding that time-delays are less sensitive to substructure than flux-ratios and require a less complex modelling.

Here, we have restricted the analysis to double lens systems. Such systems have fewer constraints than quads, nevertheless the advantage is that they can be described in terms of simpler models with fewer parameters. This is not the case for quad lenses in

which the quadrupole structure induces an internal shear that needs to be taken into account to correctly describe the lens time-delay. The lens reconstruction technique described in Alard (2007, 2008) and adapted in Habara & Yamamoto (2011) could be particularly useful in this case especially in combination with the Bayesian selection approach described here to determine the order of the perturbative lens reconstruction. Though, such technique may present difficulties since in most cases we do not see arcs but only point-like images.

The number of known lensed quasars which are potentially good targets for time-delay measurements is currently of order a hundred. In the future such dataset will increase thanks to numerous survey programs. The use of the Bayesian model selection we have discussed can provide large homogeneous subsample of lenses that are suitable for unbiased cosmological parameter inference. In particular, along the line of Parkinson & Liddle (2010), using Markov Monte Carlo Chain techniques one could perform a Bayesian model averaging of cosmological parameters over homogeneous subsamples of lenses each described by a class of lens models.

## ACKNOWLEDGEMENTS

We thank A.R. Liddle, D. Sluse, J. Wambsganss, C.R. Keeton and S.H. Suyu for their valuable comments and the anonymous referee who has helped us to improve and enrich the content of this paper. I. Balmès is supported by a scholarship of the “Ministère de l’Éducation Nationale, de la Recherche et de la Technologie” (MENRT). The research leading to these results has received funding from the European Research Council under the European Community’s Seventh Framework Programme (FP7/2007-2013 Grant Agreement no. 279954).

## REFERENCES

- Alard, C., 2007, MNRAS, 382, L58
- Alard, C., 2008, MNRAS, 388, 375
- Auger, M.W., Fassnacht, C.D., Wong, K.C., Thompson, D., Matthews, K., Soifer, B.T., 2008, ApJ, 673, 778
- Bassett, B.A., Corasani, P.S., Kunz, M., 2004, ApJ, 617, L1
- Blandford, R., Narayan, R., 1986, ApJ, 310, 568
- Biggs, A.D. et al., 1999, MNRAS, 304, 349
- Binney, J., Tremaine, S., 1987, Galactic Dynamics, Princeton Univ. Press, Princeton
- Browne, I.W.A., Patnaik, A.R., Walsh, D., Wilkinson, P.N., 1993, MNRAS, 263, L32
- Burud, I. et al., 2000, ApJ, 544, 117
- Burud, I. et al., 2002, A&A, 383, 71
- Burud, I. et al., 2002, A&A, 391, 481
- Chavez, R. et al., 2012, MNRAS, 425, L56
- Coe, D., Moustakas, L.A., 2009, ApJ, 706, 45
- Cohen, J.G., Lawrence, C.R., Blandford, R.D., 2003, ApJ, 583, 67
- Colley, W.N. et al., ApJ, 587, 71
- Cornish, N.J., Littenberg, T.B., 2007, PRD, 76, 083006
- Courbin, F., Lidman, C., Frye, B.L., Magain, P., Broadhurst, T.J., Pahre, M.A., Djorgovski, S.G., 1998, ApJ, 499, L119
- D’Agostini, G., 2005, arXiv:physics/0511182.
- Dai, X. & Kochanek, C.S., 2005, ApJ, 625, 633
- Dai, X. & Kochanek, C.S., 2009, ApJ, 692, 677

- Dobke, B.M., King, L.J., Fassnacht, C.D., Auger, M.W., 2009, MNRAS, 397, 311
- Giovi, F., Amendola, L., 2001, MNRAS, 325, 1097
- Goicoechea, L.J., Gil-Merino, R., Ullán, A., 2005, MNRAS, 360, L60
- Gregory, P., 2005, Bayesian Logical Data Analysis for the Physical Sciences, Cambridge Univ. Press, Cambridge
- Gregory, P.C., Fischer, D.A., 2010, MNRAS, 403, 731
- Fischer, P., Schade, D., Barrientos, L.F., 1998, ApJ, 503, L127
- Ford, E.B., Gregory, P.C., 2007, ASPC, 371, 189
- Haarsma, D.B., Hewitt, J.N., Lehar, J., Burke, B.F., 1999, ApJ, 510, 64
- Habara, Y., Yamamoto, K., 2011, IJMPD, 20, 371
- Holder, G.P., Schechter, P.L., 2003, ApJ, 589, 688
- Jaffe, A., 1996, ApJ, 471, 24
- Jakobsson, P., Hjorth, J., Burud, I., Letawe, G., Lidman, C., Courbin, F., 2005, A&A, 431, 103
- Jeffreys, H., 1961, Theory of Probability, 3rd edn. Oxford Univ. Press, Oxford
- Jullo, E., 2007, New Journal of Physics, 9, 447
- Keeton, C.R., 2011, Astrophysics Source Code Library, 2003
- Keeton, C.R., Kochanek, C.S., Seljak, U., 1997, ApJ, 482, 604
- Keeton, C.R., Gaudi, B.S., Petters, A.O., 2003, ApJ, 598, 138
- Kneib, J., Cohen, J.G., Hjorth, J., 2000, ApJ, 544, L35
- Kochanek, C.S., 1991, ApJ, 373, 354
- Kochanek, C.S., 2002, ApJ, 578, 25
- Kochanek, C.S., Falco, E.E., Impey, C., Lehar, J., McLeod, B., Rix, H.-W., 2008, <http://www.cfa.harvard.edu/castles/>
- Koopmans, L.V.E., 2005, MNRAS, 363, 1136
- Koopmans, L.V.E., de Bruyn, A.G., Jackson, N., 1998, MNRAS, 295, 534
- Koptelova, E. et al., 2012, arXiv:1204.5396
- Larson, D. et al., 2011, ApJS, 192, 16L
- Lehár, J. et al., 2000, ApJ, 536, 584
- Liddle, A.R. et al., 2007, astro-ph/0703285
- Linder, E., 2011, arXiv:1109.2592
- Lovell, J.E.J. et al., 1998, ApJ, 508, L51
- MacKay, D.J., 2003, Information Theory, Inference and Learning Algorithms, Cambridge University Press, Cambridge
- Marshall, P.J., Hobson, M.P., Slosar, A., 2003, MNRAS, 346, 489
- Meylan, G., Courbin, F., Lidman, C., Kneib, J.-P., Tacconi-Garman, L.E., 2005, A&A, 438, 37
- Mukherjee, P., Parkinson, D., Liddle, A.R., 2006, ApJL, 638, L51
- Mukherjee, P. et al., 2006, MNRAS, 369, 1725
- Oguri, M., 2006, MNRAS, 367, 1241
- Oguri, M., 2007, ApJ, 660, 1
- Oguri, M., Marshall, P.J., 2010, MNRAS, 405, 2579
- Oguri, M., Taruya, A., Suto, Y., Turner, E.L., ApJ, 2002, 568, 488.
- Oguri, M., et al., 2005, ApJ, 622, 106
- Oguri, M., Keeton, C.R., Dalal, N., 2005, MNRAS, 364, 1451
- Paraficz, D., Hjort, J., 2009, A&A, 507, L49
- Paraficz, D., Hjort, J., 2010, ApJ, 712, 1378
- Paraficz, D., Hjorth, J., Elíasdóttir Á., 2009, arXiv, 0903.1027
- Parkinson, D., Liddle, A.R., 2011, PRD, 82, 103533
- Petters, A.O., Levine, H., Wambsgans, J., Singularity Theory and Gravitational Lensing, 2001, Birkhäuser, Boston
- Poindexter, S., Morgan, N., Kochanek, C.S., Falco, E.E., 2007, ApJ, 660, 146
- Press, W.H., 1996, IAU Sym.173: Astrophysical Applications of Gravitational Lensing, 173, 407
- Refsdal, S., 1964, MNRAS, 128, 307
- Refsdal, S., 1966, MNRAS, 132, 101
- Rusin, D., Kochanek, C.S., Keeton, C.S., 2003, ApJ, 595, 29
- Saha, P., Williams, L.L.R., 1997, MNRAS, 292, 148
- Saha, P. et al., 2006, ApJ, 650, L17
- Saini, T.D., Weller, J., Bridle, S.L., 2004, MNRAS, 348, 603
- Salucci, P. et al., 2007, MNRAS, 378, 41
- Schild, R.E., Smith, R.C., 1991, AJ, 191, 813
- Schneider, P., Ehlers, J., Falco, E.E., 1991, Gravitational Lenses, Springer, Berlin
- Schneider, P., Kochanek, C., Wambsgans, J., 2006, in Meylan, G., Jetzer, P., North, P., eds, Gravitational Lensing: Strong, Weak and Micro: Saas-Fee Advanced Course, Springer, Berlin
- Shalyapin, V.N. et al., 2009, MNRAS, 397, 1982
- Sluse, D. et al., 2012, A&A, 544, A62
- Suyu, S.H., 2012, MNRAS, 426, 868
- Suyu, S.H., Marshall, P.J., Hobson, M.P., Blandford, R.D., 2006, MNRAS, 371, 983
- Suyu, S.H. et al., 2009, ApJ, 691, 277S
- Suyu, S.H. et al., 2010, ApJ, 711, 201
- Treu, T., Koopmans, L.V.E., 2002, MNRAS, 337, L6
- Treu, T. et al., 2006, ApJ, 640, 662; Erratum: Treu, T. et al., 2006, ApJ, 650, 121.
- Trotta, R., 2007, MNRAS, 378, 72
- Ullán, A., Goicoechea, L.J., Zheleznyak, A.P., Koptelova, E., Bruevich, V.V., Akhunov, T., Burkhonov, O., 2006, A&A, 452, 25
- Vegetti, S., Koopmans, L.V.E., 2009, MNRAS, 392, 945
- Vuissoz C. et al., 2007, A&A, 464, 845
- Warren, S., Dye, S., 2003, ApJ, 590, 673
- Williams, L.L.R., Schechter, P.L., 1997, Astronomy & Geophysics, 38, 10
- Williams, L.L.R., Saha, P., 2000, ApJ, 119, 439
- Wong, K.C. et al., 2011, ApJ, 726, 84
- Wucknitz, O., Biggs, A.D., Browne, I.W.A., 2004, MNRAS, 349, 14
- York, T., Jackson, N., Browne, I.W.A., Wucknitz, O., Skelton, J.E., 2005, MNRAS, 357, 124

## APPENDIX A: MODEL WITH EXTERNAL SHEAR

In this Appendix we present a derivation of the time-delay and magnification equations respectively in the case of a power-law potential with external shear. The latter reads as

$$\psi(\theta) = \frac{b^2}{3-n} \left(\frac{\theta}{b}\right)^{3-n} - \gamma \frac{\theta^2}{2} \cos 2(\phi - \phi_\gamma). \quad (\text{A1})$$

We can relate one of the model parameters to the remaining ones using the lens equation, since both images result of the same source at  $\beta$ . This gives us the following equation:

$$|\beta(\theta_A)|^2 = |\beta(\theta_B)|^2 \quad (\text{A2})$$

which can be rewritten, using the lens equation  $\beta = \theta - \nabla\psi(\theta)$ , as a second order equation in  $X = b^{n-1}$ :

$$UX^2 + 2VX + W = 0 \quad (\text{A3})$$

with

$$U = \theta_A^{2(2-n)} - \theta_B^{2(2-n)} \quad (\text{A4})$$

$$V = \theta_B^{3-n}(1 + \gamma C_B) - \theta_A^{3-n}(1 + \gamma C_A) \quad (\text{A5})$$

$$W = \theta_A^2(1 + 2\gamma C_A + \gamma^2) - \theta_B^2(1 + 2\gamma C_B + \gamma^2) \quad (\text{A6})$$

where  $C_{A,B} = \cos 2(\phi_{A,B} - \phi_\gamma)$ . Assuming that  $\theta_A \geq \theta_B$  and  $n > 1$ , and using the usual notation  $\Delta = V^2 - UW$  we have the following solutions: for  $\Delta > 0$

$$b^{n-1} = \frac{-V + \sqrt{\Delta}}{U}, \quad (\text{A7})$$

the solution  $b^{n-1} = \frac{-V - \sqrt{\Delta}}{U}$  is eliminated since it does not reduce to the right value for  $\gamma = 0$  (note however that it would be the correct solution if  $n < 1$ ). Note also that for  $n = 1$ , there is no parameter  $b$  and this equation has no meaning; for  $\Delta = 0$ , the solution is simply

$$b^{n-1} = \frac{-W}{2V}, \quad (\text{A8})$$

while for  $\Delta < 0$ , there are no real solutions and the lens cannot be described for this combination of  $n$ ,  $\gamma$  and  $\phi_\gamma$ . Having reduced the number of lens model parameters the time delay between images A and B can be computed using the value of  $t_A$  and  $t_B$ :

$$t_i = (1 + z_l) \frac{D_l D_s}{D_{ls}} \left[ \frac{1}{2} |\nabla \psi|^2 + \psi(\theta_i) \right], \quad (\text{A9})$$

where we have used the lens equation  $\beta - \theta_i = -\nabla \psi(\theta_i)$ . In the case of the magnification we have for each image:

$$\mu_i^{-1} = \left[ 1 - \left( \frac{\theta_i}{b} \right)^{1-n} \right] \left[ 1 - (2-n) \left( \frac{\theta_i}{b} \right)^{1-n} \right] \quad (\text{A10})$$

$$+ (1-n) \gamma C_i \left( \frac{\theta_i}{b} \right)^{1-n} - \gamma^2, \quad (\text{A11})$$

and the flux ratio is simply given by  $F_{AB} = \mu_A / \mu_B$ .

## APPENDIX B: LENS DATA ASTROMETRY

In table B1 we report the astrometric data of the positions of images (A,B) and lens (L) for all lenses used in the lens data analysis. The references to the data are listed in table 1.

**Table B1.** Astrometry for all lenses used in the data analysis

lens	object	$\Delta\alpha$	$\Delta\delta$
B0218+357	L	$\equiv 0$	$\equiv 0$
	A	$-0.250 \pm 0.005$	$-0.125 \pm 0.007$
B1600+434	B	$0.057 \pm 0.006$	$0.001 \pm 0.008$
	L	$\equiv 0 \pm 0.05$	$\equiv 0 \pm 0.05$
FBQ 0951+2635	A	$-0.33 \pm 0.01$	$1.09 \pm 0.01$
	B	$0.07 \pm 0.01$	$-0.24 \pm 0.01$
HE 1104-1805	G	$0.760 \pm 0.003$	$-0.455 \pm 0.003$
	A	$\equiv 0$	$\equiv 0$
HE 2149-2745	B	$0.900 \pm 0.003$	$-0.635 \pm 0.003$
	G	$0.974 \pm 0.003$	$-0.510 \pm 0.004$
PKS 1830-211	A	$\equiv 0$	$\equiv 0$
	B	$2.901 \pm 0.003$	$-1.332 \pm 0.003$
Q0142-100	G	$0.714 \pm 0.007$	$1.150 \pm 0.005$
	A	$\equiv 0$	$\equiv 0$
Q0957+561	B	$0.890 \pm 0.003$	$1.446 \pm 0.003$
	G	$0.498 \pm 0.004$	$-0.456 \pm 0.004$
SBS 0909+532	A	$\equiv 0$	$\equiv 0$
	B	$0.649 \pm 0.001$	$-0.724 \pm 0.001$
SBS 1520+530	G	$1.764 \pm 0.003$	$-0.574 \pm 0.003$
	A	$\equiv 0$	$\equiv 0$
SDSS J1206+4332	B	$2.145 \pm 0.003$	$-0.613 \pm 0.003$
	G	$1.406 \pm 0.006$	$-5.027 \pm 0.005$
SDSS J1650+4251	A	$\equiv 0$	$\equiv 0$
	B	$1.229 \pm 0.005$	$-6.048 \pm 0.004$
SDSS J1650+4251	G	$0.415 \pm 0.125$	$-0.004 \pm 0.081$
	A	$\equiv 0$	$\equiv 0$
SDSS J1650+4251	B	$0.987 \pm 0.003$	$-0.498 \pm 0.003$
	G	$1.141 \pm 0.003$	$-0.395 \pm 0.003$
SDSS J1650+4251	A	$\equiv 0$	$\equiv 0$
	B	$1.429 \pm 0.003$	$-0.652 \pm 0.003$
SDSS J1650+4251	G	$-0.664 \pm 0.137$	$1.748 \pm 0.028$
	A	$\equiv 0 \pm 0.011$	$\equiv 0 \pm 0.010$
SDSS J1650+4251	B	$-0.098 \pm 0.006$	$2.894 \pm 0.009$
	G	$0.017 \pm 0.032$	$-0.872 \pm 0.026$
SDSS J1650+4251	A	$\equiv 0$	$\equiv 0$
	B	$0.223 \pm 0.002$	$-1.163 \pm 0.001$